

Interface magnetic anisotropy in cobalt clusters embedded in a platinum or niobium matrix.

M. Jamet¹, M. Négrier¹, V. Dupuis¹, J. Tuaillon-Combes¹, P. Mélinon¹, A. Pérez¹, W. Wernsdorfer², B. Barbara², J. Vogel² and B. Baguenard³

¹ *Département de Physique des Matériaux, Université Claude Bernard-Lyon 1 et CNRS, 69622 Villeurbanne, FRANCE.*

² *Laboratoire Louis Néel, CNRS, 38042 Grenoble, FRANCE.*

³ *Laboratoire de Spectrométrie ionique et moléculaire, Université Claude Bernard Lyon 1 et CNRS, 69622 Villeurbanne, FRANCE.*

(October 30, 2018)

A low concentration of cobalt clusters with a fcc structure and containing almost one thousand atoms are embedded in two different metallic matrices: platinum and niobium. Samples have been prepared using a co-deposition technique. Cobalt clusters preformed in the gas phase and matrix atoms are simultaneously deposited on a silicon substrate under Ultra High Vacuum (UHV) conditions. This original technique allows to prepare nanostructured systems from miscible elements such as Co/Pt and Co/Nb in which clusters keep a pure cobalt core surrounded with an alloyed interface. Magnetic measurements performed using a Vibrating Sample Magnetometer (VSM) reveal large differences in the magnetic properties of cobalt clusters in Pt and Nb pointing out the key role of cluster/matrix interfaces.

PACS numbers: 75.50.Tt, 61.46.+w, 75.30.Gw

I. INTRODUCTION

Magnetic nanostructures are subjects of growing interest on account of their potential applications in the fields of high density magnetic recording media and spin electronics. Indeed, using magnetic clusters (containing from a few hundreds to a few thousand atoms) as memory bits should highly increase the storage density. However, clusters with a large magnetic anisotropy have to be used in this case to overcome the superparamagnetic limit¹. Cobalt clusters embedded in a platinum matrix could be good candidates because Co/Pt multilayers display very large perpendicular magnetic anisotropy (PMA)². Despite the nearly spherical shape of clusters, a large remaining interface magnetic anisotropy is expected. Therefore, this system would allow to increase the particle blocking temperature up to temperatures compatible with magnetic recording applications. In the same time, we are investigating the magnetic properties of individual cobalt clusters using a new microSQUID technique³ to rule out any statistical treatment of the experimental data (taking into account size, shape or defects distributions). Note that Co/Nb multilayers are also used in superconducting spin valve devices⁴. For these reasons, a detailed study of Co clusters embedded

in a superconducting niobium matrix is reported in a previous paper⁵. Though cobalt clusters have similar structures in Co/Pt and Co/Nb systems (a pure cobalt core and an alloyed interface), we observe that their magnetic properties are drastically different. In the present paper, we first report a detailed magnetic study of the Co/Pt system showing an anomalous dependence of the cluster magnetization with temperature and a large interface anisotropy. Then, we compare these results with previous ones obtained with the Co/Nb system.

II. SAMPLE PREPARATION AND STRUCTURAL CHARACTERIZATION

Cobalt clusters are prepared using a laser vaporization source improved according to Milani-de Heer design⁶. The Ti:sapphire vaporization laser used provides output energies up to 300 mJ at 790 nm, for a pulse duration of 3 μ s and a 10 Hz repetition rate⁷. This source produces an intense supersonic cluster beam allowing us to grow films in the Low Energy Cluster Beam Deposition (LECBD) regime. In this case, clusters do not fragment upon impact on the substrate or in the matrix⁸. We can prepare nanostructured thin films by random stacking of incident free clusters on different substrates or films of cobalt clusters embedded in various matrices (here Pt and Nb) thanks to the co-deposition technique. This last one consists in two independent beams reaching at the same time a silicon (100) substrate tilted at 45° at room temperature: the preformed neutral cluster beam and the atomic beam used for the matrix. Depositions are performed in a UHV chamber ($p=5 \times 10^{-10}$ Torr) to limit cluster and matrix contamination. The matrix is evaporated using a UHV electron gun evaporator mounted in the deposition chamber. By controlling both evaporation rates with quartz balance monitors, we can continuously adjust the cluster concentration in the matrix. Moreover, few neutral cobalt clusters (thickness $e < 1$ monolayer) are deposited on a carbon coated copper grid and subsequently protected by a thin amorphous carbon layer on top (10 nm) to perform ex-situ High Resolution Transmission Electron Microscopy (HRTEM) observations. Nearly spherical clusters with a fcc structure and a rather sharp size distribution (mean diameter $D_m \approx 3.0$

nm, dispersion $\sigma = 0.2 - 0.3$) are observed. Actually, in order to minimize their surface energy, clusters mainly have a truncated octahedron shape⁹. A 20 nm-thick film of randomly stacked cobalt clusters on a silicon substrate is prepared to perform Grazing Incidence Small Angle X-ray Diffraction (GISAXD) measurements at LURE (Laboratoire pour l'Utilisation du Rayonnement Electromagnétique, Orsay-FRANCE). The diffraction spectrum reported in Fig. 1 clearly confirms that cobalt clusters exhibit a fcc structure with roughly the same mean diameter ($D_m \approx 3.9$ nm) as the one derived from TEM observations.

In order to investigate the crystallographic structure of cobalt clusters embedded in Pt and Nb matrices, we prepared 500 nm-thick Pt and Nb films containing a 15 % volumic concentration of clusters. We recorded and compared the GISAXD signals for two different photon energies: $h\nu = 7.7$ keV (cobalt K-edge) and $h\nu = 7$ keV in Co/Nb. For $h\nu = 7$ keV, we still observe the cobalt fcc (111) peak as in the pure cobalt cluster film (Fig. 1). Note that we previously obtained the same result for cobalt clusters embedded in a SiO_x matrix¹⁰. Unfortunately, in the particular case of Co/Pt, the X-ray contrast between Co and Pt is so large that we cannot observe the cobalt signal. As a consequence, we will assume that cobalt clusters keep their fcc structure in Co/Pt as in Co/Nb. Furthermore, previous X-ray absorption measurements (Extended X-ray Absorption Fine Structure: EXAFS) were performed at LURE on Co/Pt¹¹ (resp. Co/Nb⁵) systems. They revealed an alloying effect at the cluster surface in both Co/Pt and Co/Nb miscible systems. For magnetic measurements using a VSM apparatus, we prepared a 500 nm-thick Pt film containing a 4 % cobalt volume concentration (Co/Pt sample) and a 500 nm-thick Nb film containing a 2 % cobalt volume concentration (Co/Nb sample). Very low concentrations are chosen to rule out any magnetic coupling between particles in the sample.

III. MAGNETIC STUDY OF THE CO/PT SYSTEM

In the following, we note $M_s(T)$ the particle magnetization which is temperature dependent. This parameter is important since it gives information on the magnetic state of the particles. The magnetization is proportionnal to the saturation moment of the sample labeled $m_{sat}(T)$ through the relation:

$$m_{sat}(T) = M_s(T) \int_0^\infty N(\pi D^3/6) f(D) dD \propto M_s(T) \quad (1)$$

Particles are assumed to be nearly spherical and D is the diameter, N is the total number of particles in the sample and $f(D)$ is the log-normal magnetic size distribution with D_m the mean diameter and σ the dispersion:

$$f(D) = \frac{1}{D\sqrt{2\pi\sigma^2}} \exp\left(-\left(\ln\left(\frac{D}{D_m}\right)\right)^2 \frac{1}{2\sigma^2}\right) \quad (2)$$

Considering the narrow size distribution of clusters as deduced from TEM observations, we assume that the magnetization does not depend on the particle size in Eq. (1) (ref. 12). Moreover, in the following, we consider non-interacting particles i.e. only the applied magnetic field (\mathbf{H}_{app}) has to be taken into account. Furthermore for cobalt, the exchange length is 7 nm which is larger than the mean particle size of 3 nm. Thus, a single domain cluster can be seen as a macrospin with uniform rotation of its magnetization. Finally, we will assume a uniaxial magnetic anisotropy within the particles¹³. If the easy magnetization directions are randomly distributed and the applied magnetic field is larger than the coercive field $H_c(T)$, the magnetic moment of the sample can be written as¹:

$$m(H_{app}, T) = m_{sat}(T) \left\langle \int_0^\pi d\psi \frac{\sin\psi}{2} \frac{\int_0^\pi d\theta \sin\theta \int_0^{2\pi} d\phi \cos\alpha \exp(\eta \cos^2\theta + \xi \cos\alpha)}{\int_0^\pi d\theta \sin\theta \int_0^{2\pi} d\phi \exp(\eta \cos^2\theta + \xi \cos\alpha)} \right\rangle \quad (3)$$

Here, we use the spherical coordinates. The two angles (θ, ϕ) give the direction of the particle magnetization. The easy magnetization direction is fixed along the z axis while the magnetic field orientation given by the angle ψ between \mathbf{H}_{app} and the easy direction is continuously varied from $\psi = 0$ to $\psi = \pi$. $\cos\alpha = \sin\psi \sin\theta \sin\phi + \cos\psi \cos\theta$, $\eta = \Delta E/k_B T$ where ΔE is the energy barrier to cross in order to reverse the particle magnetization, and $\xi = \mu_0 H_{app}(\pi D^3/6) M_s(T)/k_B T$. The final expression is then averaged over the magnetic size distribution $f(D)$ according to the formula:

$$\langle \Gamma \rangle = \frac{\int_0^\infty D^3 \Gamma(D) f(D) dD}{\int_0^\infty D^3 f(D) dD} \quad (4)$$

where $\Gamma(D)$ is a function of the particle diameter. Eq. (3) simplifies in the case $\xi \gg 1$ (high field, low temperature)¹:

$$m(H_{app}, T) \approx m_{sat}(T) \left(1 - \left\langle \frac{1}{\xi} \right\rangle - \frac{4}{15} \left\langle \frac{\eta^2}{\xi^2} \right\rangle + \dots \right) \quad (5)$$

In a first approximation, we use this expansion limited to the first order as a saturation approach law to determine $m_{sat}(T)$:

$$m(H_{app}, T) \approx m_{sat}(T) \left(1 - \frac{a}{\mu_0 H_{app}} \right), \quad (6)$$

$$a = \frac{k_B T \exp(-9\sigma^2/2)}{(\pi D_m^3/6) M_s(T)}$$

Since we assume that the magnetization is independent on the applied magnetic field, we certainly give an upper limit for $m_{sat}(T)$. From the magnetization curves reported in Fig. 2, we clearly show that the saturation moment is temperature dependent. Thus the magnetization also depends on the temperature and its evolution vs. T is shown in Fig. 3. At very low temperature, the thermal fluctuations of the magnetization are negligible and we obtain a relevant information on the magnetic state of the cluster: $M_s(0K) \approx M_s(1.5K) = 1600 \pm 200 \text{ kA.m}^{-1}$. This value is larger than the cobalt bulk magnetization ($M_s^{bulk} = 1430 \text{ kA.m}^{-1}$). When the coercive field $H_c(T)$ is zero, Eq. (3) also simplifies in the case $\xi \ll 1$ (low field, high temperature), and can be written to the first order¹⁴:

$$m(H_{app}, T) \approx m_{sat}(T) \left\langle \frac{\xi}{3} \right\rangle \quad (7)$$

$$= m_{sat}(T) \frac{\mu_0 H_{app} (\pi D_m^3 / 6) M_s(T)}{3 k_B T} \exp(13.5 \sigma^2)$$

and using Eq. (1), we find:

$$m(H_{app}, T) = \frac{N(\pi D_m^3 / 6)^2 \exp(18\sigma^2)}{3 k_B} \frac{\mu_0 H_{app} M_s^2(T)}{T} \quad (8)$$

This corresponds exactly to the magnetic moment we measure in the Zero Field Cooled (ZFC) protocols when all the particles are superparamagnetic (the remanent moment of the sample being equal to zero). Thus, we deduce: $M_s(T) \propto \sqrt{T} m_{ZFC}(H_{app}, T) / \mu_0 H_{app}$ (ref. 15). In Fig. 3, we plot $\sqrt{T} m_{ZFC}(H_{app}, T) / \mu_0 H_{app}$ for 3 different applied magnetic fields. The resulting curves superimpose with the one obtained from $m_{sat}(T)$ for $T > 150$ K in the superparamagnetic regime. In this field range, we notice that the magnetization does not depend on $\mu_0 H_{app}$. In the following, the temperature dependence of the particle magnetization is systematically taken into account. We first estimate the magnetic size distribution from the highest temperature magnetization curves. At $T=300$ K and $T=250$ K, anisotropy terms can be neglected and a simple Langevin function $L(\xi)$ allows us to fit $m(H_{app}, T)$ (ref. 5) (Fig. 4):

$$\frac{m(H_{app}, T)}{m_{sat}(T)} = \frac{\int_0^\infty D^3 L(\xi) f(D) dD}{\int_0^\infty D^3 f(D) dD} \quad (9)$$

We deduce: $D_m = 2.7 \pm 0.1 \text{ nm}$ and $\sigma = 0.35 \pm 0.05$ which roughly corresponds to the size distribution obtained from TEM observations. Decreasing the temperature, anisotropy terms are no more negligible and have to be considered to fit the experimental data. To estimate them, we perform a detailed analysis of both the remanent moment vs. temperature and the ZFC magnetization curves using the magnetic size distribution previously found.

From hysteresis loops at low temperature, we deduce the remanent moment $m_r(T)$ of the sample. We do not observe a narrowing of the loops at the vicinity of $\mu_0 H_{app} = 0 \text{ T}$ below 10 K so that we can assume that almost all the cobalt particles are magnetically blocked below this temperature. Moreover, we notice that $m_r(T) \approx m_{sat}(T)/2$ which implies a uniaxial magnetic anisotropy within the particles¹⁶. In Fig. 5(a), we plot $m_r(T)/m_r(1.5K)$ and fit this curve using the following expression⁵:

$$\frac{m_r(T)}{m_r(1.5K)} = \frac{\int_{D_B(T)}^\infty D^3 f(D) dD}{\int_{D_B(1.5K)}^\infty D^3 f(D) dD} \quad (10)$$

where $D_B(T)$ is the blocking diameter of the particles at temperature T and $\mu_0 H_{app} = 0 \text{ T}$. One finds $D_B(T)$ when the relaxation time of the particle is equal to the measuring time: $\tau = \tau_0 \exp(\Delta E / k_B T) = \tau_{mes} \Leftrightarrow \Delta E = k_B T \ln(\tau_{mes} / \tau_0)$. In our case, $\tau_{mes} = 10 \text{ s}$ and the attempt frequency τ_0^{-1} is typically 10^9 - 10^{12} Hz . To fit the ratio $m_r(T)/m_r(1.5K)$, we take $\Delta E = K D^\alpha$ where K and α are free parameters. The best fitting values are given in Table I, they correspond to an interface anisotropy with $\alpha \approx 2$. We also fit the ZFC magnetization curves for different applied magnetic fields using (Fig. 5(b)):

$$\frac{m_{ZFC}(H_{app}, T)}{m_{sat}(T)} = \frac{\int_0^{D_B(H_{app}, T)} D^3 (\xi/3) f(D) dD}{\int_0^\infty D^3 f(D) dD} \quad (11)$$

Here, we neglect the blocked particle susceptibility. The blocking diameter $D_B(H_{app}, T)$ now depends on the applied magnetic field, and the anisotropy energy barrier is written: $\Delta E = K(H_{app}) D^\alpha$ where the anisotropy constant $K(H_{app})$ which may depend on the applied magnetic field and the exponent α are free parameters. The results are given in Table I for six different magnetic fields. They show that the anisotropy constant is actually independent on the magnetic field and confirm an interface anisotropy within the particles: $\alpha \approx 2$.

At intermediate temperatures: $T=200$ K and $T=150$ K, we cannot fit the magnetization curves using a simple Langevin function as shown in Fig. 6. Indeed to achieve this, one has to use Eq. (3) to take the anisotropy term into account¹⁷ (i.e. $\Delta E = K D^\alpha$). Thus we assume an interface anisotropy as previously suggested and solve numerically Eq. (3) in order to deduce the anisotropy constant. Fig. 6 shows theoretical and experimental curves, and the resulting anisotropy constants are given in Table I. From all these results we can assert that interface is responsible for the large uniaxial magnetic anisotropy in cobalt clusters embedded in a platinum matrix. Note that it was not necessary to take the temperature dependence of the anisotropy constant into account to fit the experimental data. It is now interesting to compare this system with Co/Nb.

IV. COMPARISON WITH THE CO/NB SYSTEM

Here, we summarize briefly the main results we obtained on the Co/Nb sample in a previous paper⁵. Magnetization measurements are performed at temperatures higher than 8 K because of the superconducting behavior of niobium films for $T < 7$ K. As in the case of Co/Pt, we use Eq. (6) as a saturation approach law to determine $m_{sat}(T)$ and subsequently Eq. (1) to deduce the cobalt magnetization $M_s(T)$ in the sample (Fig. 7). In the same figure, we plot $\sqrt{T} m_{ZFC}(H_{app}, T) / \mu_0 H_{app}$ for 3 different applied magnetic fields and $T < 150$ K (above this temperature the magnetic signal reaches the magnetometer resolution). We find the magnetization: $M_s = 500 \pm 50 \text{ kA.m}^{-1}$ which shows nearly no dependence on the temperature. The same magnetic measurements performed with a second sample containing a 3 % volume concentration of cobalt clusters give: $M_s = 510 \pm 60 \text{ kA.m}^{-1}$. Finally, complementary X-ray Magnetic Circular Dichroism (XMCD) was performed at the ESRF (European Synchrotron Radiation Facility, Grenoble-FRANCE). The absorption signal was recorded under a 3 Tesla magnetic field at $T = 5$ K, and we measured the total electron yield in the photon energy range which spans the L2 and L3 absorption lines of cobalt. Using the sum rules¹⁸, we can estimate the mean atomic magnetic moment of cobalt atoms: $\mu_{at} = 0.5 \pm 0.05 \mu_B$ which corresponds to $M_s = 430 \pm 50 \text{ kA.m}^{-1}$. This value is in good agreement with the previous ones. Moreover, the orbital to spin moment ratio is enhanced compared with the bulk value¹⁹ as expected in small particles: $m_L/m_S \approx 0.2$. However, one has to notice that this technique probes the first 3 nm of the sample where slight oxidation might be possible.

We note D_m^{mag} and σ^{mag} (resp. D_m^{TEM} and σ^{TEM}) the mean cluster diameter and the dispersion of the magnetic (resp. TEM) size distribution. If we assume that: $\sigma^{mag} = \sigma^{TEM}$, one can write: $M_s = M_s^{bulk}(D_m^{mag}/D_m^{TEM})^3$. By taking $M_s = 500 \pm 50 \text{ kA.m}^{-1}$ and $D_m^{TEM} = 3.0 \pm 0.1 \text{ nm}$, we find $D_m^{mag} = 2.1 \pm 0.2 \text{ nm}$. This is in rather good agreement with the magnetic size: $D_m = 2.1 \pm 0.1 \text{ nm}$, $\sigma = 0.35 \pm 0.05$ which fits really well the magnetization curves at $T = 300$ K and $T = 200$ K using the bulk magnetization (Fig. 8). We first notice a large difference between the magnetic mean diameter in Co/Pt (2.7 nm) and the one in Co/Nb (2.1 nm). In the case of Co/Nb, we conclude that at least two cobalt atomic monolayers are magnetically dead at the cluster surface (Fig. 9(a) and 9(b)) while in Co/Pt, the alloying effect is limited since we roughly find the same diameter as the one derived from TEM observations. In ref. 5 concerned with Co/Nb, we only considered a volume anisotropy K_V within cobalt clusters and found: $K_V = 2.0 \pm 0.3 \cdot 10^5 \text{ J/m}^3$. In the present work, we assume that cobalt clusters exhibit an interface anisotropy in Co/Nb to allow a comparison with Co/Pt. In this case, the anisotropy energy barrier is writ-

ten: $\Delta E = K_S D^2$. We use Eq. (10) to fit the evolution of the remanent moment vs. temperature (Fig. 10(a)) and Eq. (11) to fit the ZFC magnetization curves (Fig. 10(b)). In both cases, we find: $K_S = 0.05 \pm 0.008 \text{ mJ/m}^2$ which is almost one order of magnitude smaller than in Co/Pt.

V. DISCUSSION AND CONCLUSION

Cobalt-platinum and cobalt-niobium elements are miscible which may promote interdiffusions at the cluster/matrix interfaces. Indeed, previous structural studies^{11,5} showed that one (resp. two) cobalt atomic layer diffuses inside the Pt (resp. Nb) matrix. In this discussion we show that a simple core-shell model with a pure cobalt core surrounded with a disordered $\text{Co}_x\text{Pt}_{1-x}$ or $\text{Co}_x\text{Nb}_{1-x}$ alloyed shell can originally account for the magnetic properties of cobalt clusters embedded in both Pt and Nb matrices. A comparable model has already been suggested by Canedy *et al.*²⁰ in Co/Pt superlattices. We can write the cluster magnetization as:

$$M_s(T) = x M_s^{core}(T) + (1 - x) M_s^{shell}(T) \quad (12)$$

where x is the fraction of cobalt atoms in the core with $M_s^{core}(T) = M_s^{bulk}(T)$ ($M_s(0K) = 1430 \text{ kA.m}^{-1}$), and $(1 - x)$ the fraction of cobalt atoms in the alloyed interface shell. For the following calculations we consider the cluster model reported in Fig. 9(a) and 9(b) which contains 1289 atoms. For Co/Pt, one atomic layer is expected to diffuse inside the matrix giving $x = 0.63$. Thus one finds: $M_s(0K) = 0.63 \times 1430 + 0.37 \times M_s^{shell}(0K) = 1600 \text{ kA.m}^{-1}$ which provides: $M_s^{shell}(0K) \approx 1900 \text{ kA.m}^{-1}$. This magnetization enhancement of cobalt is much smaller than that in CoPt alloys (3325 kA.m^{-1}) (ref. 20). This may be due to dimensional effects as mentioned by Canedy *et al.*²⁰. However, the temperature dependence of the magnetization indicates that the Curie temperature of the interface (T_C) is quite small (the Curie temperature in the core is assumed to be much higher than 300 K). Besides, above this temperature the sample magnetization reaches: $M_s(T) = x M_s^{bulk}(T) \approx 0.63 \times 1430 = 901 \text{ kA.m}^{-1}$. Experimentally, that gives: $200 < T_C < 250 \text{ K}$ (Fig. 3). The low Curie temperature of CoPt disordered alloys has already been pointed out by Weller *et al.*²¹ or Devolder²².

We further annealed this sample during 10 minutes at $T = 450^\circ\text{C}$ under a vacuum of 10^{-7} Torr. In Fig. 3, we plot the sample magnetization vs. T using the saturation approach law given by Eq. (6). At 2 K, the large magnetization $M_s = 2720 \text{ kA.m}^{-1}$ now approaches the CoPt alloy value. It implies that almost all the cluster atoms have diffused inside the platinum matrix to form small alloyed "clusters". The low Curie temperature: $T_C \approx 150 \text{ K}$ confirms that there is no more pure

cobalt core in the sample ($x = 0$). Moreover, magnetization curves measured down to 2 K show no remanent moment so that the alloyed "cluster" anisotropy is negligible as expected for disordered CoPt alloys²².

For Co/Nb, two atomic layers are expected to diffuse inside the matrix thus: $x = 0.36$. If we assume that the CoNb disordered alloy is magnetically dead⁵, one finds the sample magnetization: $M_s(T) = xM_s^{bulk}(T) \approx 0.36 \times 1430 = 515 \text{ kA.m}^{-1}$, which is in good agreement with the experimental data (Fig. 7). Finally, experimental magnetization values in Co/Pt and Co/Nb samples can be well interpreted on the basis of a simple core-shell model.

In Co/Pt, we unambiguously find the existence of an interface anisotropy and it is actually impossible to fit the experimental data by only considering a volume anisotropy within the clusters. Interface anisotropy originates from the combination of the large spin-orbit coupling in Pt with the natural anisotropy directions induced by the surface². Further surface strains induced by the surrounding Pt atoms may contribute to this interface anisotropy.

Let us assume a volume anisotropy within the cobalt clusters. That leads to an anisotropy constant K_V given by the relation: $K_V V_m = K_S S_m$ where V_m and S_m are the mean cluster volume and surface respectively. Using the mean diameter D_m obtained in section III, one finds: $K_V = 6K_S/D_m \approx 7.10^5 \text{ J/m}^3$. For an infinite cobalt cylinder, shape anisotropy is equal to $\mu_0 M_s^2/4 \approx 6.4.10^5 \text{ J/m}^3$ if we use the bulk magnetization²³. This is even smaller than the above K_V value thus shape anisotropy cannot account for the experimental one. Furthermore, cubic magnetocrystalline anisotropy reported in ref. 24 ($1.2.10^5 \text{ J/m}^3$) or in ref. 25 ($2.7.10^5 \text{ J/m}^3$) are also too small to account for the experimental value. In conclusion the assumption of a volume anisotropy seems not physically obvious.

In order to compare our surface anisotropy with previous works, we can estimate the corresponding anisotropy energy per cobalt atom at the cluster surface. For this purpose, we use the cluster model in Fig. 9(c). Indeed, for a perfect truncated octahedron as the one given in Fig. 9(a) and 9(b), symmetries cancel surface anisotropy and we add one (111) facet to break this symmetry. We note K^{at} the atomic anisotropy energy. Summing over all the cluster surface atoms, one finds the anisotropy energy in the whole particle: $E = -15K^{at}\cos^2(\theta)$ where θ is the angle between the magnetization and the [111] direction. Dividing by the cluster surface, we can deduce K^{at} from the experimental anisotropy: $K^{at} \approx 3 \text{ meV/at}$. This is one order of magnitude larger than the experimental values given in ref. 2, 26, 27 ranging between 0.1 and 0.3 meV/at for 1-2 cobalt monolayers in Co/Pt multilayers. However, comparisons with Co/Pt multilayers are quite difficult because this is more a two-dimensional problem whereas clusters involve a three-dimensional treatment. Concerning Co/Nb, we believe that interface anisotropy is so small that it becomes possible to fit the magne-

tization curves using a volume anisotropy. But recent works performed on single cobalt clusters³ embedded in a niobium matrix show that interface still rules magnetic anisotropy in this system.

Other

experimental issues to increase magnetic anisotropy in nanosized particles and consequently the corresponding blocking temperature could be tested in the near future: using another matrix element to increase spin-orbit coupling at the cluster surface, preparing slightly elongated particles since interface anisotropy is proportional to the deformation...

VI. ACKNOWLEDGEMENTS

The authors would like to thank Professor C. BINNS from the Department of Physics and Astronomy-University of Leicester-UK, for his help during the XMCD measurements on the ID12B line at the ESRF.

-
- ¹ J. L. Dormann, D. Fiorani, and E. Tronc, *Advances in Chemical Physics* (I. Prigogine and Stuart Rice, p. 288, 1997) Vol. XCVIII.
 - ² N. Nakajima, T. Koide, T. Shidara, H. Miyauchi, H. Fukutani, A. Fujimori, K. Iio, and T. Katayama, *Phys. Rev. Lett.* **81**, 5229 (1998).
 - ³ M. Jamet, W. Wernsdorfer, C. Thirion, D. Mailly, V. Dupuis, P. Mélinon, and A. Pérez, cond-mat/0012029.
 - ⁴ A. Buzdin, A. Vedyayev, and N. Ryzhanova, *Europhys. Lett.* **48**, 686 (1999).
 - ⁵ M. Jamet, V. Dupuis, P. Mélinon, G. Guiraud, A. Pérez, W. Wernsdorfer, A. Traverse, and B. Baguenard, *Phys. Rev. B* **62**, 493 (2000).
 - ⁶ P. Milani and W. A. de Heer, *Rev. Sci. Instrum.* **61**, 1835 (1990).
 - ⁷ M. Pellarin, E. Cottancin, J. Lermé, J. L. Vialle, J. P. Wolf, M. Broyer, V. Paillard, V. Dupuis, A. Pérez, J. P. Pérez, J. Tuaillon, and P. Mélinon, *Chem. Phys. Lett.* **224**, 338 (1994).
 - ⁸ A. Pérez, P. Mélinon, V. Dupuis, P. Jensen, B. Prével, M. Broyer, M. Pellarin, J. L. Vialle, and B. Palpant, *J. Phys. D* **30**, 709 (1997).
 - ⁹ J. Buttet, and J. P. Borel, *Helvetica Physica Acta* **56**, 541 (1983).
 - ¹⁰ J. Tuaillon, Ph. D. Thesis, Villeurbanne, France, 1995.
 - ¹¹ M. Négrier, J. Tuaillon, V. Dupuis, P. Mélinon, A. Pérez, and A. Traverse (unpublished).
 - ¹² I. M. L. Billas, A. Chatelain, and W. A. de Heer, *Science* **265**, 1682 (1994).
 - ¹³ This assertion is justified in the next sections. A biaxial magnetic anisotropy should be a more general case. But the main difference only comes from the reversal path: the

- magnetization preferentially rotates perpendicularly to the hard magnetization axis in the case of a biaxial anisotropy.
- ¹⁴ K. Muller, and F. Thurley, *Int. J. Mag.* **5**, 203 (1973).
 - ¹⁵ G. Xiao, and C. L. Chien, *J. Appl. Phys.* **61**, 3308 (1987).
 - ¹⁶ H. Pfeiffer, *Phys. Stat. Sol. (a)* **118**, 295 (1990).
 - ¹⁷ M. Hanson, C. Johansson, and S. Morup, *J. Phys.:Condens. Matter* **5**, 725 (1993).
 - ¹⁸ B. T. Thole, P. Carra, F. K. Sette, and G. Van Der Laan, *Phys. Rev. Lett.* **68**, 1943 (1992).
 - ¹⁹ D. A. Eastham, and I. W. Kirkman, *J. Phys.: Condens. Matter* **12**, 525 (2000).
 - ²⁰ C. L. Canedy, X. W. Li, and G. Xiao, *Phys. Rev. B* **62**, 508 (2000).
 - ²¹ D. Weller, H. Brändle, G. Gorman, C.-J. Lin, and H. Notarys, *Appl. Phys. Lett.* **61**, 2726 (1992).
 - ²² T. Devolder, *Phys. Rev. B* **62**, 5794 (2000).
 - ²³ A. Aharoni, *Introduction to the Theory of Ferromagnetism* (Oxford Science Publications, p. 115, 1996).
 - ²⁴ C. H. Lee, Hui He, F. J. Lamelas, W. Vavra, C. Uher, and Roy Clarke, *Phys. Rev. B* **42**, 1066 (1990).
 - ²⁵ J. P. Chen, C. M. Sorensen, K. J. Klabunde, and G. C. Hadjipanayis, *J. Appl. Phys.* **76**, 6676 (1994).
 - ²⁶ B. Hillebrands, and J. R. Dutcher, *Phys. Rev. B* **47**, 6126 (1993).
 - ²⁷ C.-J. Lin, G. L. Gorman, C. H. Lee, R. F. C. Farrow, E. E. Marinero, H. V. Do, H. Notarys, and C. J. Chien, *J. Magn. Mater.* **93**, 194 (1991).

FIG. 1. (a) Diffraction pattern (GISAXD) obtained on a 20 nm-thick film of randomly stacked cobalt clusters (crosses). Supported clusters clearly exhibit a fcc structure. (b) XRD spectra obtained on a 500 nm-thick niobium film containing a 15 % volume concentration of cobalt clusters for two different photon energies: $h\nu = 7.7$ keV (cobalt K-edge) (solid line) and $h\nu = 7$ keV (empty circles). Even embedded in a niobium matrix cobalt clusters still exhibit a fcc structure.

FIG. 2. Magnetization curves obtained for isolated cobalt clusters embedded in a platinum matrix (Co/Pt sample). Dots: experimental data, solid lines: approach to saturation simulated using Eq. (6). At $T=1.5$ K, in the ferromagnetic regime, the saturation moment is much higher than the one at $T=300$ K, in the superparamagnetic regime showing the large dependence of the magnetization on temperature.

FIG. 3. Experimental magnetization of the as-prepared and annealed Co/Pt sample estimated using Eq. (6) as a saturation approach law (full circles). In the as-prepared sample, a core-shell cluster model with a pure cobalt core and an alloyed $\text{Co}_x\text{Pt}_{1-x}$ interface well accounts for the temperature dependence of the sample magnetization. We can deduce the interface Curie temperature: $200 < T_C < 250$ K. In the annealed sample, the Curie temperature is approximately 150 K and $M_s(0\text{K})$ is much larger than in the as-prepared sample. We also plot $\sqrt{T} m_{ZFC}(H_{app}, T)/\mu_0 H_{app}$ which is proportional to M_s in the superparamagnetic regime for three different applied magnetic fields: $\mu_0 H_{app} = 10$ mT; 12.5 mT and 15 mT (full squares). The three curves superimpose with the magnetization curve obtained from the saturation approach for $T > 150$ K.

FIG. 4. Experimental magnetization curves in the superparamagnetic regime ($T=250$ K: full squares, $T=300$ K: full circles) for the Co/Pt sample. These curves are easily fitted using a simple Langevin function (solid lines) which gives the magnetic size distribution of cobalt clusters: $D_m = 2.7 \pm 0.1$ nm and $\sigma = 0.35 \pm 0.05$.

FIG. 5. (a) Experimental temperature dependence of the remanent moment (full circles) in the Co/Pt sample. The corresponding fitting curve (solid line) gives α and K in the anisotropy energy barrier (see Table I): $\Delta E = KD^\alpha$. (b) Experimental Zero Field Cooled (ZFC) magnetization curves given for 6 different applied magnetic fields. The fitting curves (solid lines) allow us to deduce α and K in the anisotropy energy barrier (see Table I).

FIG. 6. (a) Experimental magnetization curve at $T=150$ K (full squares) obtained for the Co/Pt sample. A simple Langevin function (dashed line) does not allow to fit the experimental data since the cluster anisotropy is no more negligible. Assuming an interface anisotropy, we can fit m/m_{sat} (solid line) and deduce the anisotropy constant K (see Table I). (b) Experimental magnetization curve at $T=200$ K (full squares). A simple Langevin function (dashed line) does not allow to fit the experimental data since the cluster anisotropy is no more negligible. Assuming an interface anisotropy, we can fit m/m_{sat} (solid line) and deduce the anisotropy constant K (see Table I).

FIG. 7. Experimental dependence of the magnetization vs. temperature using Eq. (6) as a saturation approach law (full circles) obtained for the Co/Nb sample. Note that the magnetization is nearly independent on temperature in this system. We also plot $\sqrt{T} m_{ZFC}(H_{app}, T)/\mu_0 H_{app}$ which is proportional to $M_s(T)$ in the superparamagnetic regime for three different applied magnetic fields: $\mu_0 H_{app} = 10$ mT; 15 mT and 20 mT (full squares). The different curves superimpose for $T > 50$ K in the superparamagnetic regime..

FIG. 8. Experimental magnetization curves in the superparamagnetic regime ($T=200$ K: full squares, $T=300$ K: full circles) for the Co/Nb sample. These curves are easily fitted using a simple Langevin function (solid lines) which gives the magnetic size distribution of the clusters: $D_m=2.1\pm0.1$ nm and $\sigma=0.35\pm0.05$.

FIG. 9. (a) Model of cluster containing 1289 atoms with a truncated octahedron shape. (111) and (100) facets allow to minimize the cluster surface energy. (b) View along a [110] direction of the cobalt cluster. From the comparison of the magnetic size distribution with the TEM one, it seems that at least 2 atomic monolayers are magnetically dead at the cluster surface in Co/Nb. (c) Model of cluster containing 1337 atoms. Dark atoms belonging to the (111) facet are added to a perfect truncated octahedron basis of 1289 atoms (light atoms) in order to break the cluster symmetry.

FIG. 10. (a) Experimental temperature dependence of the remanent moment in the Co/Nb sample (full circles). Assuming an interface anisotropy, the resulting fitting curve (solid line) gives the anisotropy constant K_S . (b) Experimental Zero Field Cooled (ZFC) magnetization curves obtained for 6 different applied magnetic fields. The fitting curves (solid lines) allow us to deduce K_S .

TABLE I. α exponent and magnetic anisotropy constant K deduced from three different experimental measurements performed on the Co/Pt sample: remanent moment vs. temperature, Zero Field Cooled (ZFC) magnetization curves and magnetization curves at intermediate temperatures (see text). They give the anisotropy energy barrier: $\Delta E = K D^\alpha$ to cross in order to reverse the magnetization of a cobalt cluster with a diameter D .

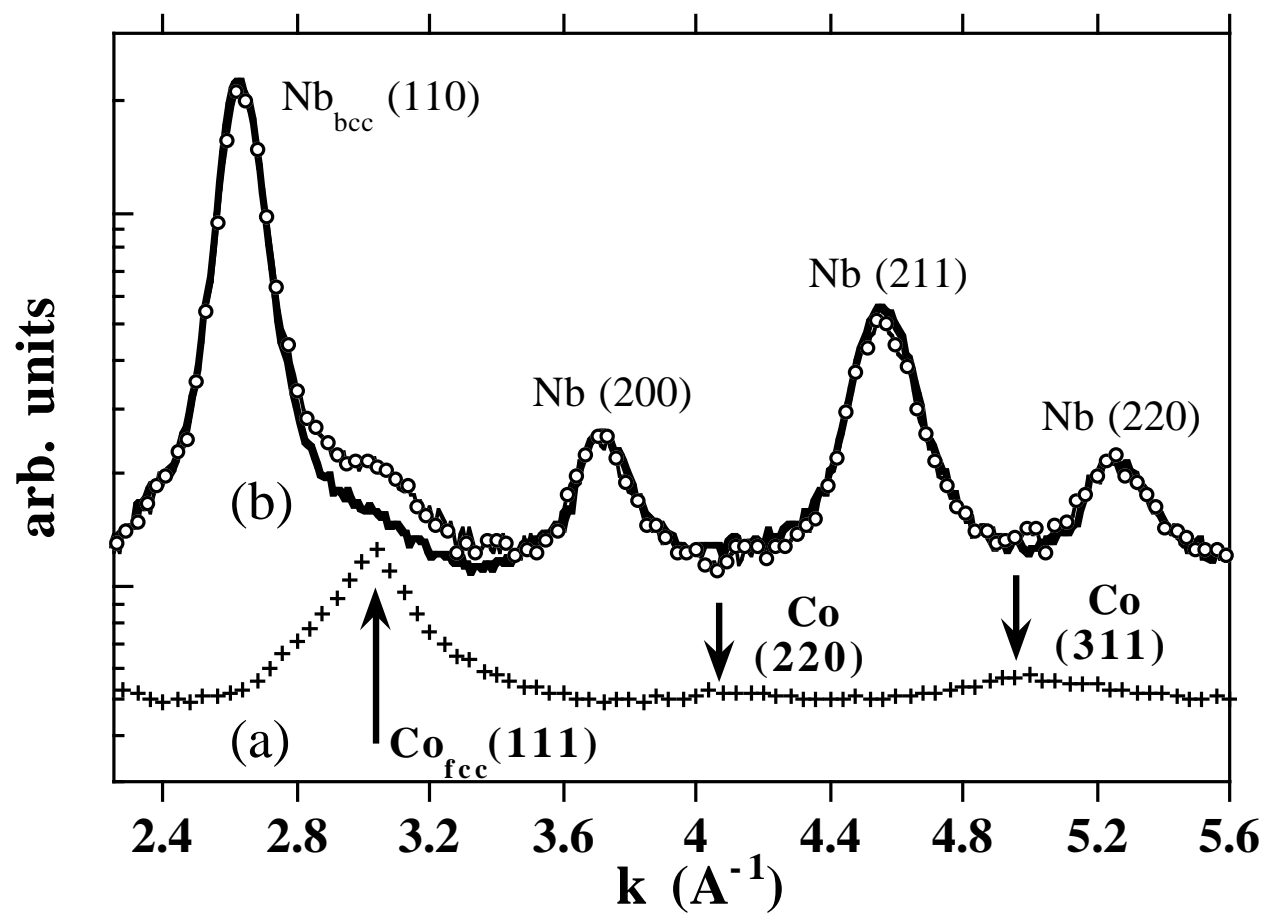


Fig. 1.

jamet *et al.*

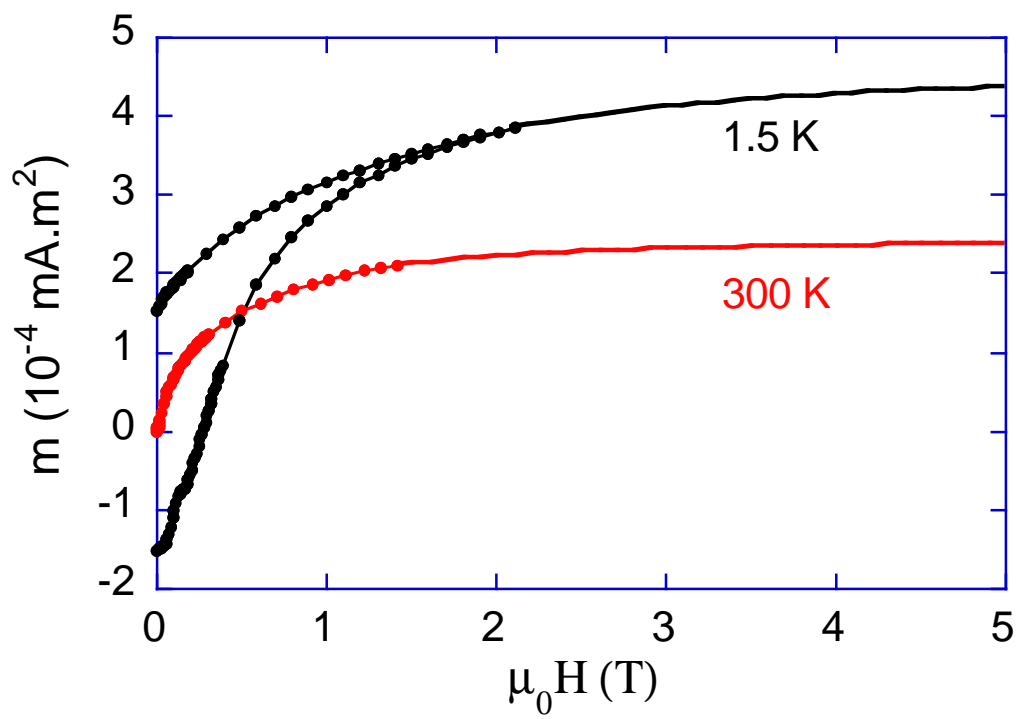


Fig. 2.

jamet *et al.*

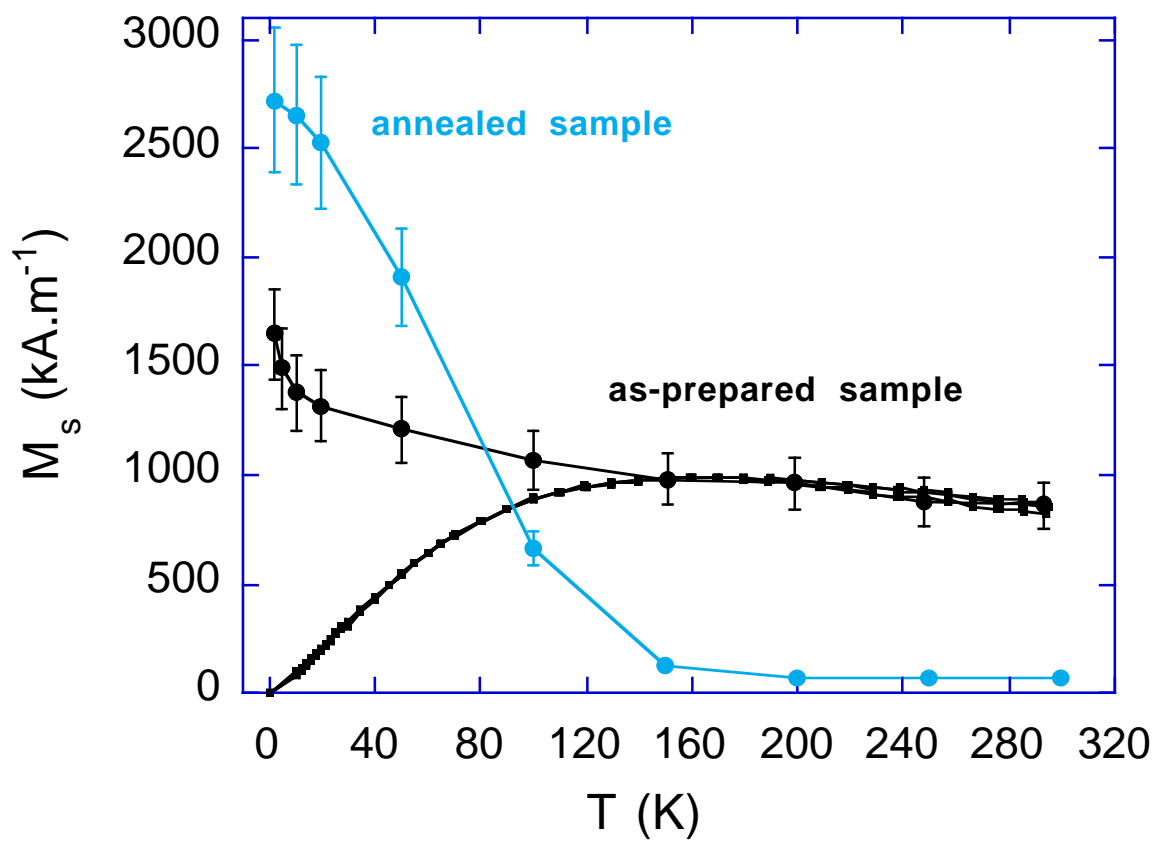


Fig. 3.

jamet *et al.*

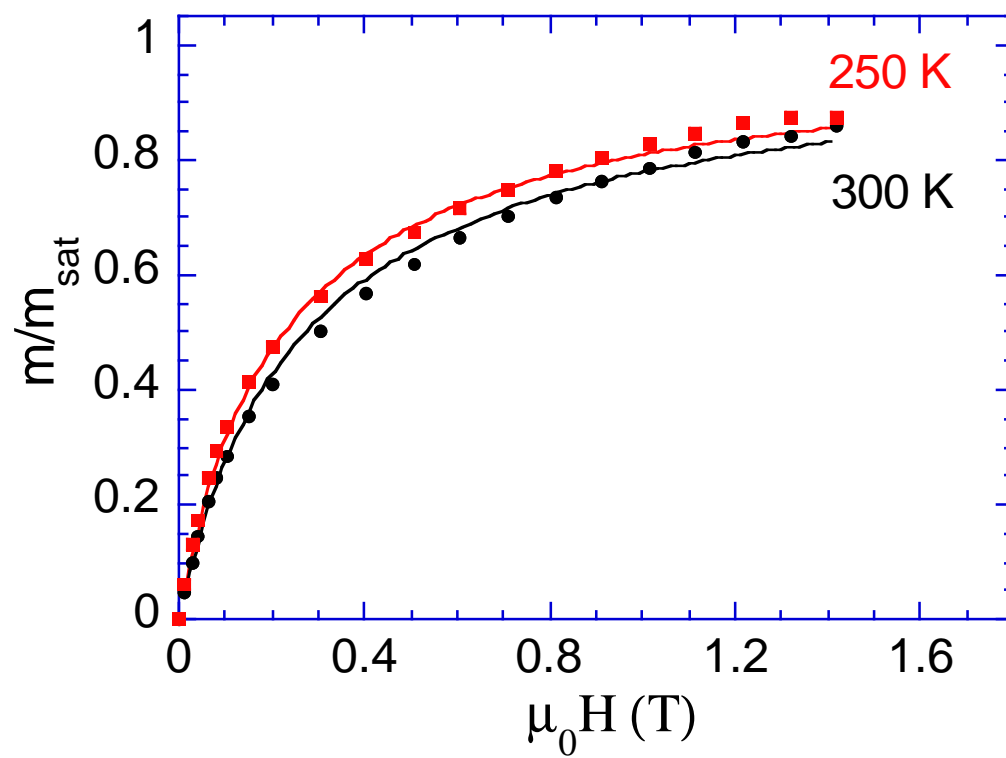


Fig. 4.

jamet *et al.*

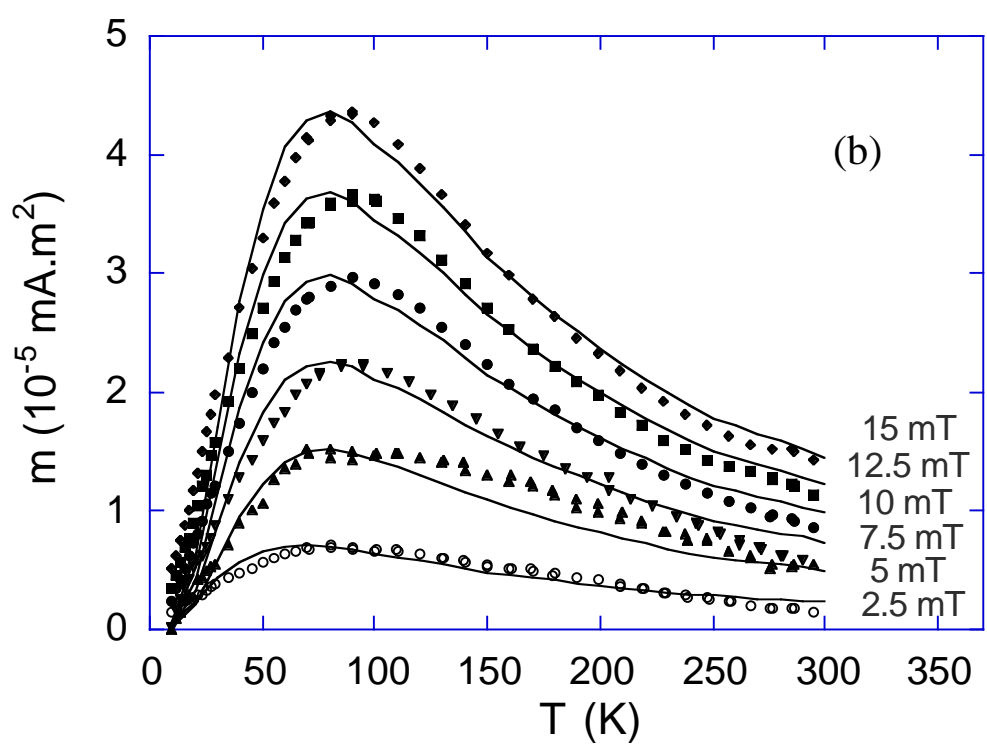
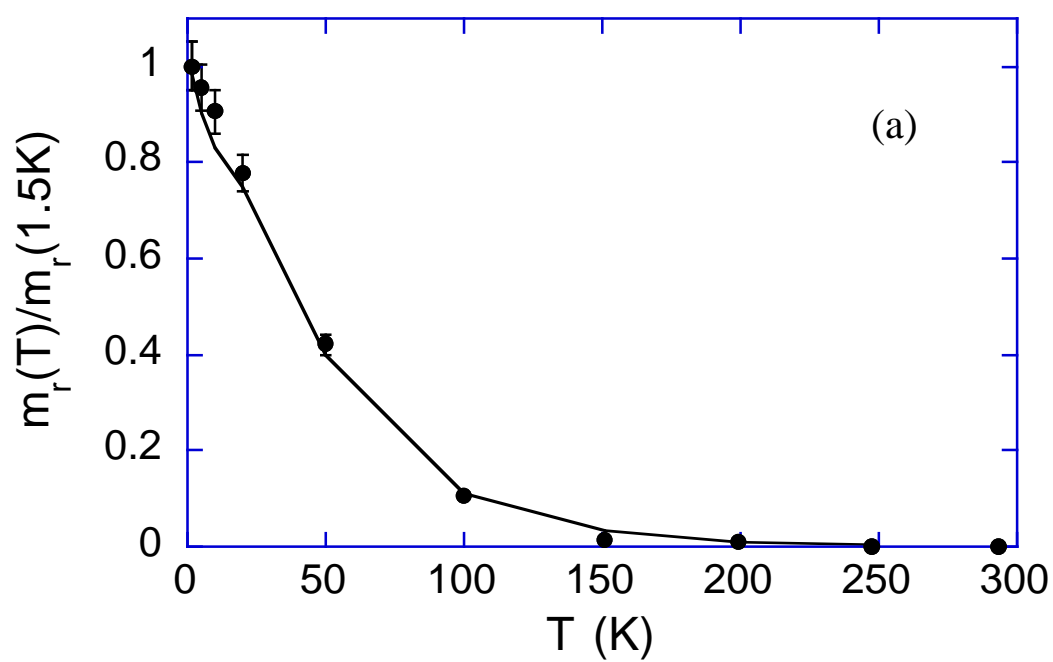
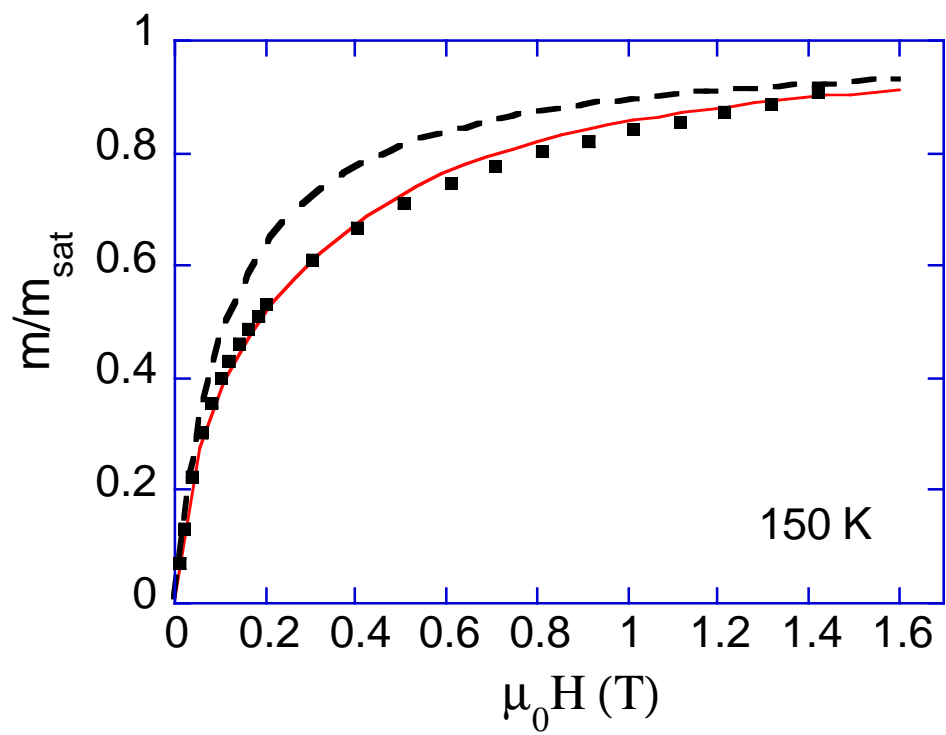
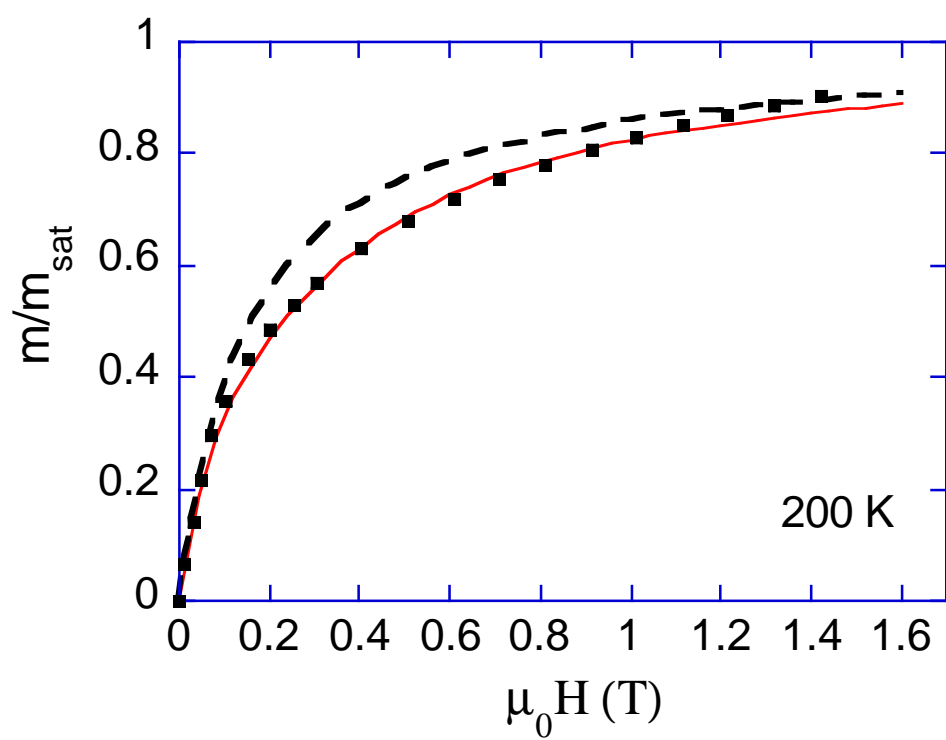


Fig. 5.

jamet et al.



(a)



(b)

Fig. 6.

jamet *et al.*

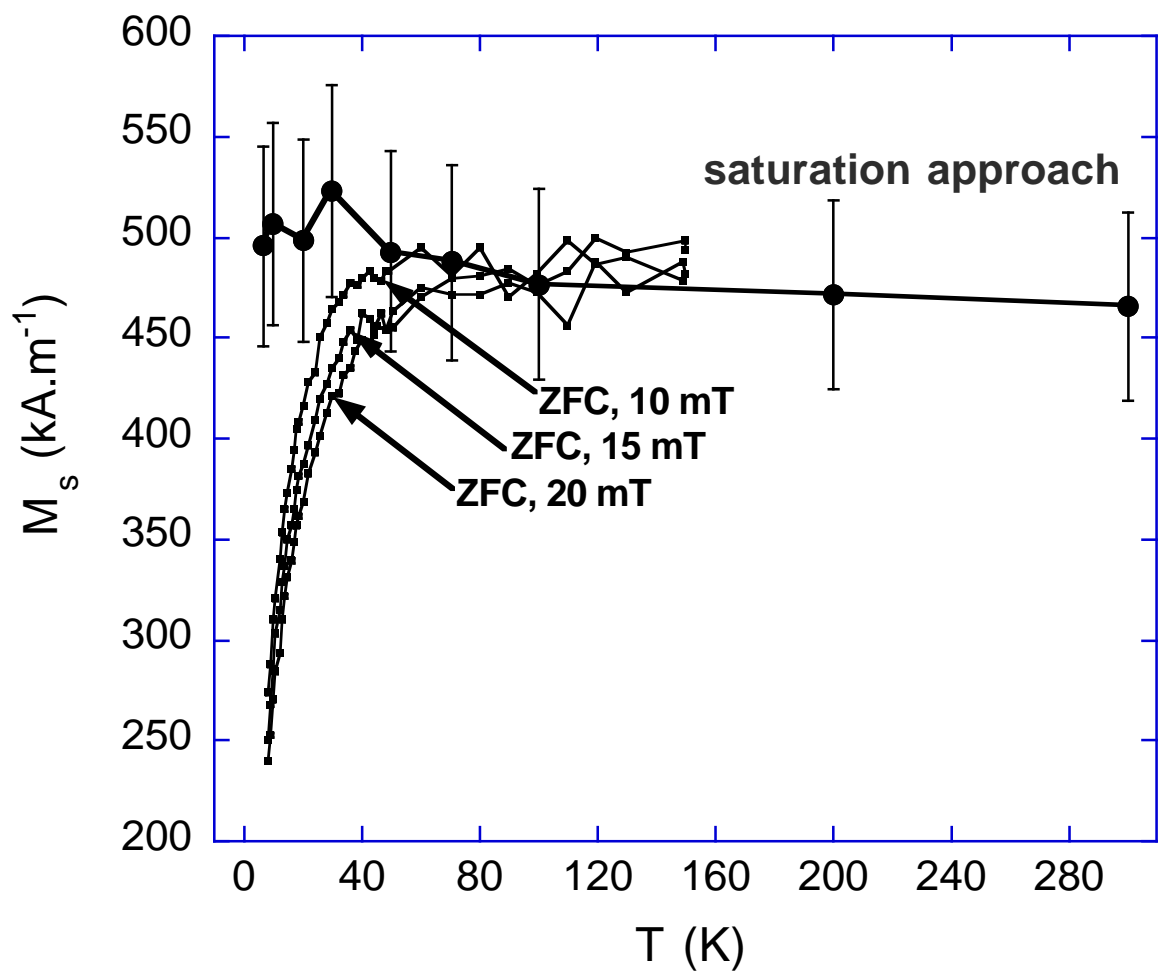


Fig. 7.

jamet *et al.*

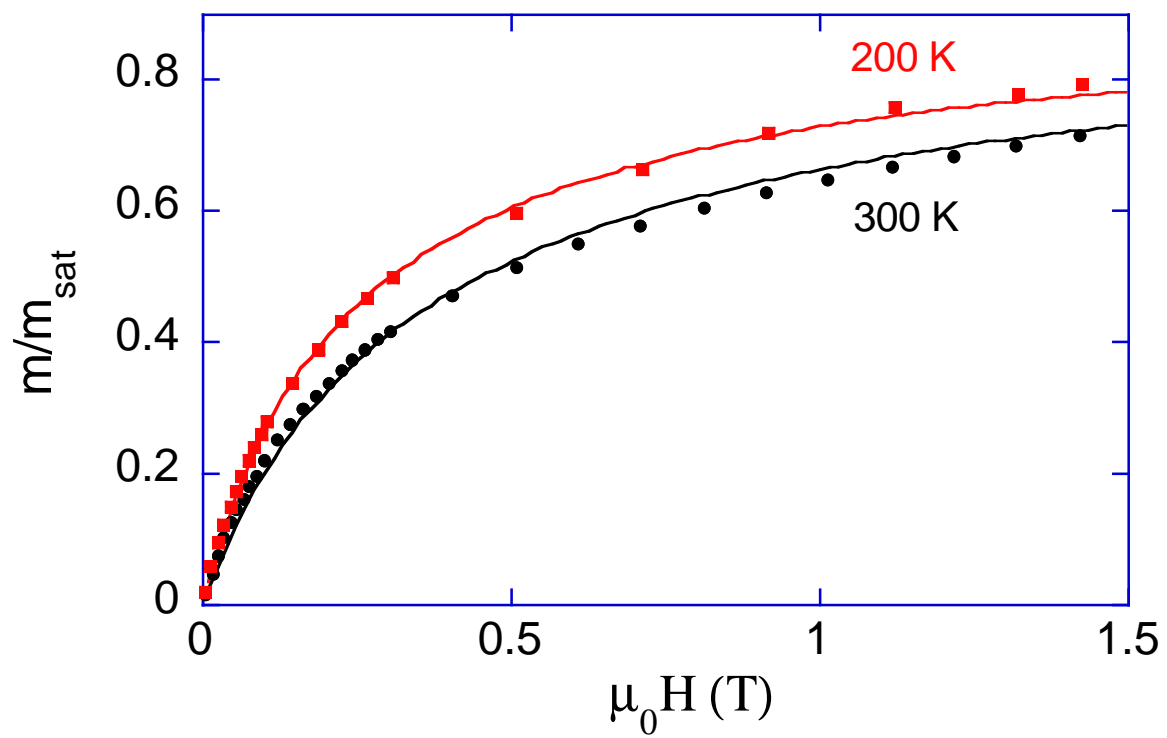
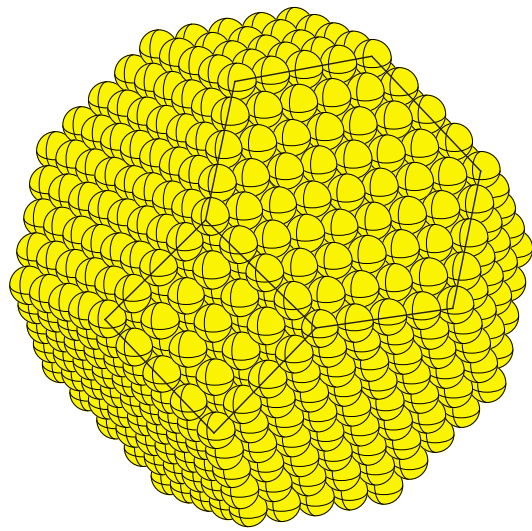


Fig. 8.

jamet *et al.*

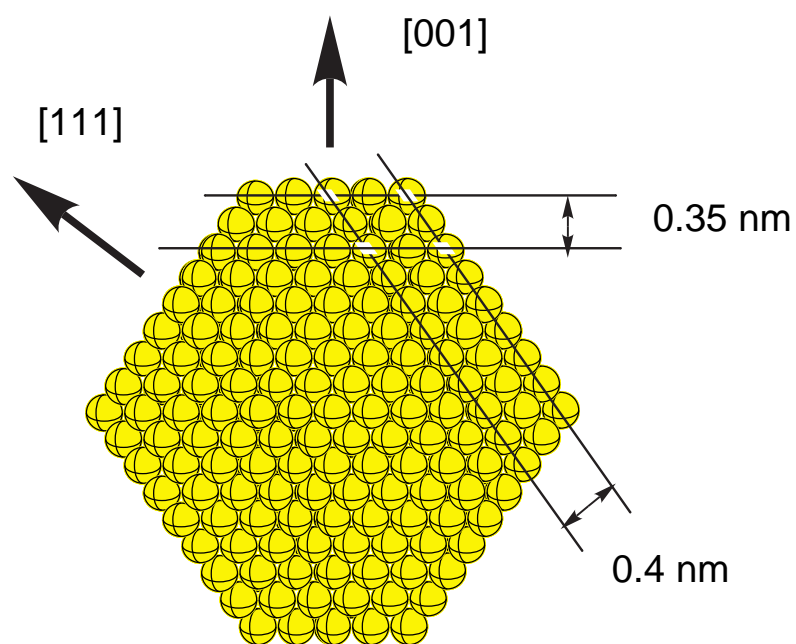
1289 atoms



(a)

Fig. 9(a).

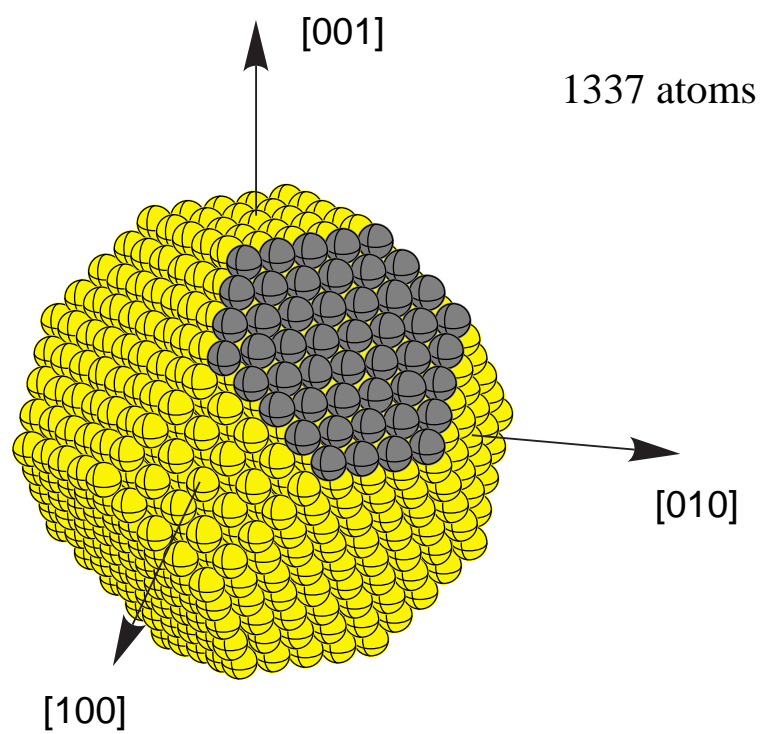
jamet *et al.*



(b)

Fig. 9(b).

jamet *et al.*



(c)

Fig. 9(c).

jamet *et al.*

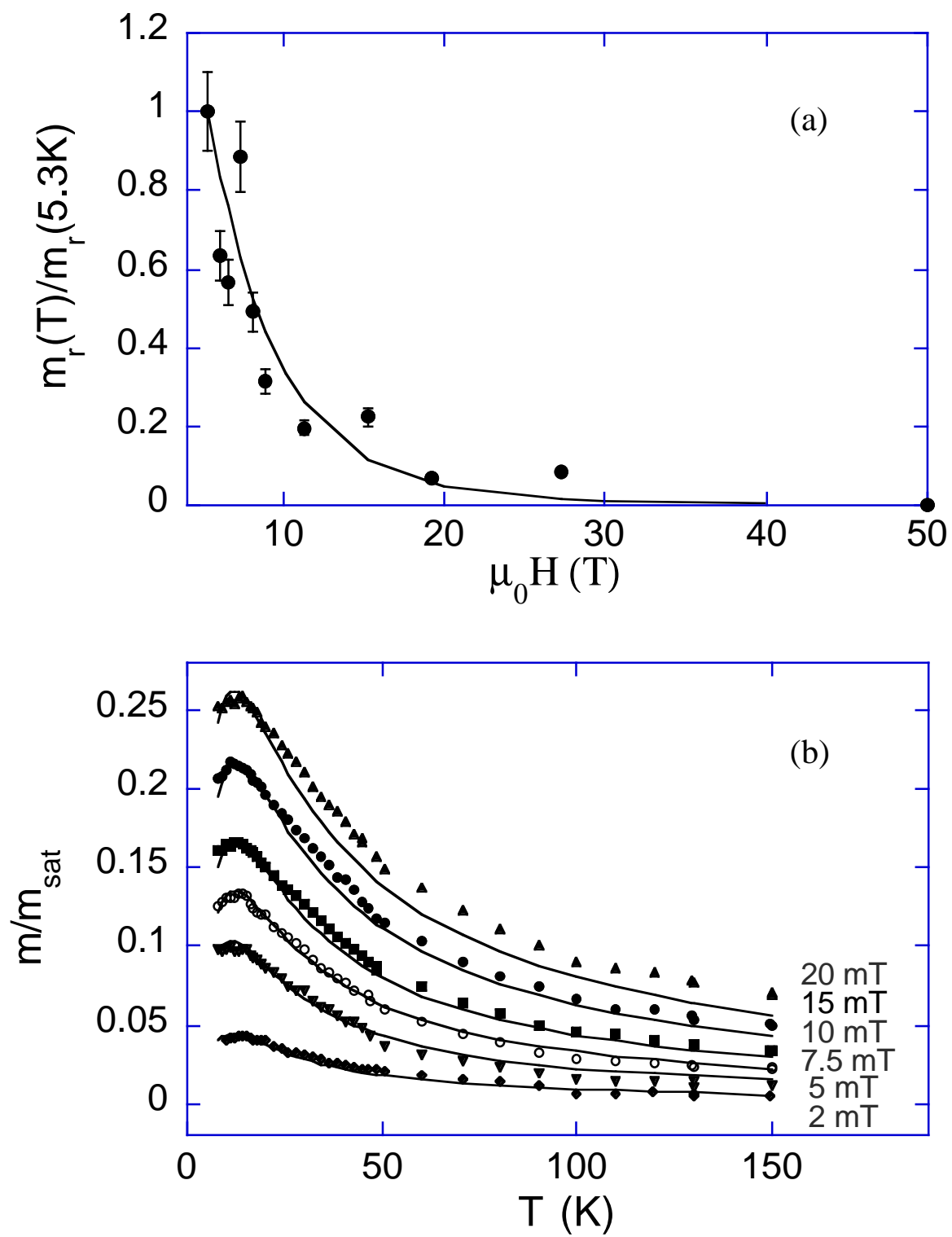


Fig. 10.

jamet et al.

	remanent	ZFC magnetization curves						magnetization curves	
	moment	2.5 mT	5 mT	7.5 mT	10 mT	12.5 mT	15 mT	T=150 K	T=200 K
α	2.0	2.3	1.9	1.9	1.9	1.9	1.9	2.0 (fixed)	2.0 (fixed)
K (mJ.m ⁻²)	0.3	0.2	0.3	0.3	0.3	0.3	0.3	0.3	0.3

Table I

jamet *et al.*